



1 **Loss of nitrogen via anaerobic ammonium oxidation (anammox) in** 2 **the California current system during the Quaternary**

3 Zoë R. van Kemenade¹, Zeynep Erdem¹, Ellen C. Hopmans¹, Jaap S. Sinninge Damsté^{1,2}, Darci Rush¹

4 ¹ NIOZ Royal Netherlands Institute for Sea Research, PO Box 59, 1790 AB, Den Burg, The Netherlands

5 ² Department of Earth Sciences, Utrecht University, Princetonlaan 8a, 3584 CB, Utrecht, the Netherlands

6 *Correspondence to:* Zoë R. van Kemenade (zoe.van.kemenade@nioz.nl)

7 **Abstract.** The California current system (CCS) hosts one of the largest oxygen minimum zones (OMZs) in the world: the
8 Eastern North Pacific (ENP) OMZ, which is dissociated into a subtropical and tropical region (i.e., the ESTNP and ETNP).
9 In the modern ENP OMZ, bioavailable nitrogen (N) is lost via denitrification and anaerobic ammonium oxidation
10 (anammox). Even so, paleo-reconstructions of N-loss have focused solely on denitrification. Fluctuations in bulk
11 sedimentary $\delta^{15}\text{N}$ over glacial-interglacial cycles have been interpreted to reflect variations in denitrification rates in
12 response to ETNP OMZ intensity changes. This $\delta^{15}\text{N}$ signal is thought to be transported northwards to the ESTNP OMZ.
13 Here, we present the first CCS sedimentary record of ladderane lipids, biomarkers for anammox, located within the ESTNP
14 OMZ (32°N; 118°W). Over the last two glacial terminations (~160 cal ka BP), ladderane concentrations were analysed in
15 combination with the index of ladderanes with five cyclobutane moieties (NL₅), short-chain (SC) ladderane degradation
16 products, and productivity proxies. This shows that: 1) ladderanes derived from anammox bacteria living within the ESTNP
17 OMZ water column; 2) ladderanes were continuously present, with relatively high concentrations during both glacial- and
18 interglacial-periods, showcasing the ESTNP OMZ must have retained an anoxic core in which N-loss occurred; and 3)
19 anammox abundance appears to have been driven both by OM-remineralization and advection changes, which regulated
20 nutrient and oxygen levels. Our study shows that anammox was an important feature in the CCS and provides a more holistic
21 picture of N-loss dynamics and the development of the ESTNP OMZ over glacial-interglacial cycles. Lastly, ladderanes
22 were also detected in 160–500 cal ka BP sediments (15.7–37.5 mbsf; analysed at a low temporal resolution), highlighting
23 their potential as anammox biomarkers in relatively deeper buried sediments for future studies.

24 **1 Introduction**

25 The California current system (CCS) is one of four major Eastern Boundary upwelling systems (EBUS). In EBUS, wind-
26 driven offshore advection of surface waters causes deeper, cold, nutrient-rich waters to be upwelled into the photic zone,
27 fuelling primary productivity (e.g., Bakun and Nelson, 1991). Consequently, the CCS is one of the world's most productive
28 oceanic regions, with year-round upwelling, resulting in high primary production rates (Huyer, 1983; Dorman and Winant,
29 1995). In the CCS, the respiration of sinking organic matter (OM), in combination with limited ventilation of the North
30 Pacific intermediate waters (Reid and Mantyla, 1978; Sonnerup et al., 1999; Fine et al., 2001), results in the formation of the



31 Eastern North Pacific oxygen minimum zone (ENP OMZ). The ENP is divided into the Eastern tropical North Pacific
32 (ETNP; 0–25°N; 75–180°W) and Eastern subtropical North Pacific (ESTNP; 25–52°N; 75–180°W) OMZs.

33 The suboxic/anoxic conditions of OMZs cause the marine nitrogen (N) cycle to shift towards two processes that
34 result in the loss of bioavailable N through the production of dinitrogen gas (N₂): 1) anaerobic ammonium oxidation
35 (anammox) and 2) denitrification. Anammox is the oxidation of ammonium (NH₄⁺) to N₂ using NO₂⁻ as the terminal electron
36 acceptor (van de Graaf et al., 1997, 1995), and is performed in the marine water column by anammox bacteria of the genus
37 ‘*Ca. Scalindua*’ (Kuypers et al., 2003). Anammox bacteria are chemolithoautotrophs and use carbon dioxide (CO₂) as their
38 carbon source. Denitrification is the stepwise reduction of nitrate (NO₃⁻), to nitrite (NO₂⁻), to N₂ (Kuenen and Robertson,
39 1987) and is performed by a wide range of organisms, most of which are heterotrophs. During denitrification, nitrous oxide
40 (N₂O) can be released as an intermediate product (Kuenen and Robertson, 1987), which has a global warming potential 265
41 times that of CO₂ (Vallero, 2019).

42 While permanent OMZs contribute to only 8 % of the total oceanic area (Paulmier and Ruiz-Pino, 2009), they are
43 responsible for 20–50 % of total global N loss (Gruber, 2004; Codispoti et al., 2001). Decreased N availability in OMZs may
44 limit primary producers, and hence, the uptake of CO₂ into the organic matter (OM) pool. This may reduce the efficiency of
45 the ocean’s biological pump, which exports organic C from the euphotic zone to the sea floor. Thus, OMZs not only have a
46 disproportionately large impact on the marine nitrogen cycle, but changes in N-loss dynamics may also feed back into the
47 carbon cycle.

48 The ENP OMZ is expanding both vertically (shoaling towards the ocean’s surface; Bograd et al., 2008) and
49 horizontally (Zhou et al., 2022) with present-day climate change. This follows observed trends of overall deoxygenation of
50 the North Pacific since the 1960’s (Whitney et al., 2007; Stramma et al., 2010; Pierce et al., 2012; Smith et al., 2022), linked
51 to anthropogenically-induced ocean warming as a response to increased greenhouse gas emissions (Laffoley and Baxter,
52 2019). As a result of the decreasing dissolved oxygen (DO) concentrations, denitrification has been shown to increase in the
53 North Pacific over the last decades (Peters et al., 2018; White et al., 2019). Vertical expansion and intensification of the ENP
54 OMZ have also occurred in the absence of anthropogenic influences in the past, as recorded by redox-sensitive trace metals
55 in the sedimentary archive (Wang et al., 2020). This is thought to be caused by changes in DO concentrations during glacial-
56 interglacial transitions (terminations). Model simulations indicate that during glacials, cooling of the polar regions led to a
57 more restrained and intensified Hadley cell (Nicholson and Flohn, 1981). This is thought to have caused southward transport
58 of high-oxygen, nutrient-rich North Pacific Intermediate Water (NPIW; Herguera et al., 2010) and limited northward
59 advection of the warm, oxygen-poor California undercurrent (CU; Fig. 1), resulting in a more oxygenated OMZ. During
60 interglacials, the oxygen deficiency in the OMZ is thought to have increased due to enhanced advection of the warm,
61 oxygen-depleted waters of the CU originating from the tropics (Lembke-Jene et al., 2018; Hendy and Kennett, 2003), water



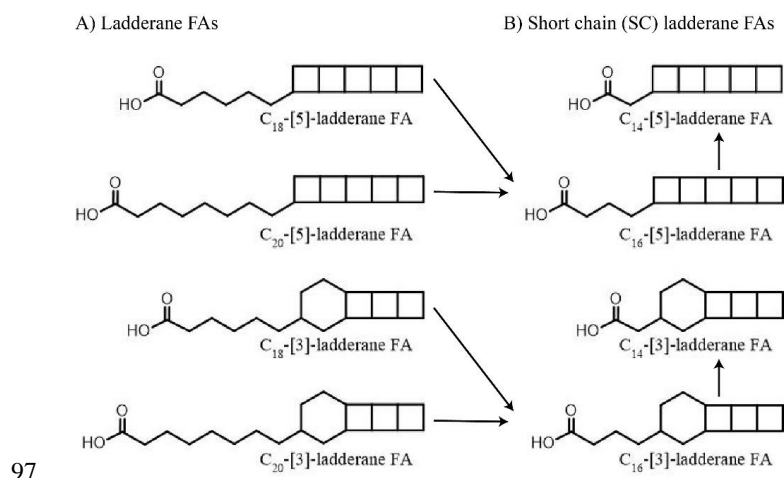
62 column stratification (Wang et al., 2020), and enhanced upwelling of nutrient-rich waters (Choumiline et al., 2019). These
63 previous glacial-interglacial transitions may be considered as analogues for the effect of future climate change on the N-
64 cycle.

65 In the CCS, enriched isotope ratio values of bulk sedimentary nitrogen ($\delta^{15}\text{N}$) during interglacial periods have been
66 interpreted to reflect increased denitrification in response to OMZ intensification (e.g., Kienast et al., 2002; Kemp et al.,
67 2003; Liu et al., 2005). Sedimentary $\delta^{15}\text{N}$ values are governed by the isotopic fractionation (ϵ) induced by biological
68 transformations and can be used to infer past N-cycling. For water column denitrification, the production of N_2 induces an
69 isotope fractionation effect of +20 to +30 ‰ on the residual nitrogen (Ryabenko, 2013; Sigman and Fripiat, 2019).
70 Enrichment cultures of anammox have, however, recently shown that *Ca. Scalindua* spp. also induces an isotope
71 fractionation effect of +16 to +30 ‰ (Kobayashi et al., 2019). Although anammox occurs in the modern North Pacific
72 oxygen deficient waters (Rush et al., 2012a; Peng et al., 2015; Sollai et al., 2015; Hamasaki et al., 2018), and anammox is
73 reported to be the dominant N-loss process in the Eastern Tropical South Pacific (ESTP; Galán et al., 2009; Thamdrup et al.,
74 2006; Hamersley et al., 2007), to the best of our knowledge, there are no reconstructions on the occurrence of anammox in
75 the sediment archive of the CCS. Moreover, a long-standing conundrum is the discrepancy between the timing of enriched
76 $\delta^{15}\text{N}$ values, and enhanced marine productivity, especially north of the ETNP (Kienast et al., 2002), suggesting a decoupling
77 between remineralization rates and N-loss (Ganeshram et al., 2000).

78 While sedimentary $\delta^{15}\text{N}$ values are shaped by the sum of N-cycling processes, lipid biomarkers provide more
79 detailed information (see Rush and Sinninghe Damsté, 2017 for a review). Anammox bacteria biosynthesise C_{18} and C_{20}
80 ladderane fatty acids (FAs) (Fig. 2). These unique lipids contain three or five linearly concatenated cyclobutane rings ([3]-
81 ladderane and [5]-ladderane, respectively; Sinninghe Damsté et al., 2002). Ladderanes have been successfully applied to
82 trace abundances of *Ca. Scalindua* spp. in the modern ENP water column (Rush et al., 2012a; Sollai et al., 2015) and as
83 anammox biomarkers in sedimentary records up to 140 ka (Jaeschke et al., 2009; Rush et al., 2019; van Kemenade et al.,
84 2023). Moreover, during exposure to oxic conditions ladderane FAs undergo microbially-mediated oxic degradation of the
85 alkyl side chain by β -oxidation, in which C_{18} - and C_{20} -ladderane FAs are sequentially transformed into the short-chain (SC)
86 C_{16} - and C_{14} -ladderane partial degradation products (Rush et al., 2011, 2012b). Thus, SC-ladderane FAs in the sediment
87 archive may be used to trace back anammox cell material that has been exposed to oxic conditions, such as sedimentation
88 through the oxic water underlying an OMZ. Furthermore, the index of ladderane FAs with five cyclobutane rings (NL_5) has
89 been shown to correlate with the *in situ* water temperature at which ladderane FAs are synthesised (Ratray et al., 2010),
90 which has been used to determine the provenance of ladderane lipids (Jaeschke et al., 2009; Rush et al., 2012a; Van
91 Kemenade et al., 2022).



92 Here, we describe the occurrence of ladderane FAs in a ~160 cal ka BP sediment record from the CCS, covering the
93 two most recent glacial terminations (T1 and T2). We combined (SC-)ladderanes and the NL₅ index with sedimentary bulk
94 δ¹⁵N, stable carbon isotope ratio (δ¹³C), total organic C (TOC) and total N (TN) to investigate the feedback of changing
95 OMZ intensity on the occurrence of anammox within the CCS. Moreover, ladderane FAs were also investigated, albeit in
96 low-resolution, in >160 cal ka BP sediments (up to 500 cal ka BP) to explore their preservation potential.



98 **Figure 1:** Structures of anammox lipid biomarkers used in this study: A) ladderane fatty acids (FAs) with 5 or 3 cyclobutane moieties
99 containing 18 or 20 carbon atoms. B) short chain ladderane fatty acids (FAs) with 5 or 3 cyclobutane moieties containing 16 or 14 carbon
100 atoms. Proposed diagenetic pathways are indicated using black arrows (adapted from Rush et al., 2011).

101 2 Hydrographic setting

102 The northern boundary of the CCS is at the transition zone between the North Pacific Current (NPC) and Alaska gyres
103 (~50°N) and is bordered in the south by the subtropical waters of Baja California, Mexico (~15–25°N). The CCS (Fig. 2A) is
104 shaped by: (i) the equatorward California current (CC), extending roughly 1000 km off the North American coast (Checkley
105 and Barth, 2009), (ii) the poleward, near-shore flowing California undercurrent (CU), and (iii) the seasonal poleward flowing
106 Davidson current (DC). The CC is a year-round, cold, low-salinity, nutrient-rich surface current (<300 m below sea surface;
107 mbss), originating from the North Pacific Current. While the CC is strongest in spring and summer, the DC originating
108 around Point Conception (35°N) dominates the surface-flow throughout winter. The deeper waters of the CC are shaped by
109 the NPIW (300–800 mbss), which circulates clockwise in the North Pacific gyre (Sverdrup et al., 1942) and is carried
110 southwards by the CC. Around Baja California, it convolutes with unventilated intermediate waters of tropical origin, which
111 have been transported to the eastern Pacific by the Equatorial undercurrent (EUC; Reid, 1997; Reid and Mantyla, 1978).
112 Here, part of the CC turns north to become the California undercurrent (CU). The CU (~100–300 mbss) carries the warm,



113 high-salinity, low oxygen waters from Baja California towards Vancouver Island (Thomson and Krassovski, 2010). Within
114 the CCS, the geostrophic flow of the CC in combination with Ekman transport and eddy activity cause an offshore transport
115 of (sub-)surface waters and strong coastal jets, which are replaced by the upwelling of the nutrient-rich undercurrent waters
116 (Huyer, 1983; Chavez and Messié, 2009). Upwelling occurs year-round, and results in high primary production (Bograd et
117 al., 2009). In the CCS, the high organic matter flux, together with the poor ventilation of the intermediate-water mass (Reid
118 and Mantyla, 1978; Fu et al., 2018), results in the formation of the ENP OMZ, disassociated in the ETNP (0–25°N; 75–
119 180°W) and ESTNP (25–52°N; 75–180°W). Dissolved oxygen (DO) concentrations in the cores ($<20 \mu\text{mol kg}^{-1}$) of both the
120 ETNP (~320–740 meters below sea surface, ‘mbss’) and ESTNP (~850–1080) OMZ decrease below $<1 \mu\text{mol kg}^{-1}$ (Palmier
121 and Ruiz-Pino, 2009).

122 **3 Methods**

123 **3.1 Sampling location and strategy**

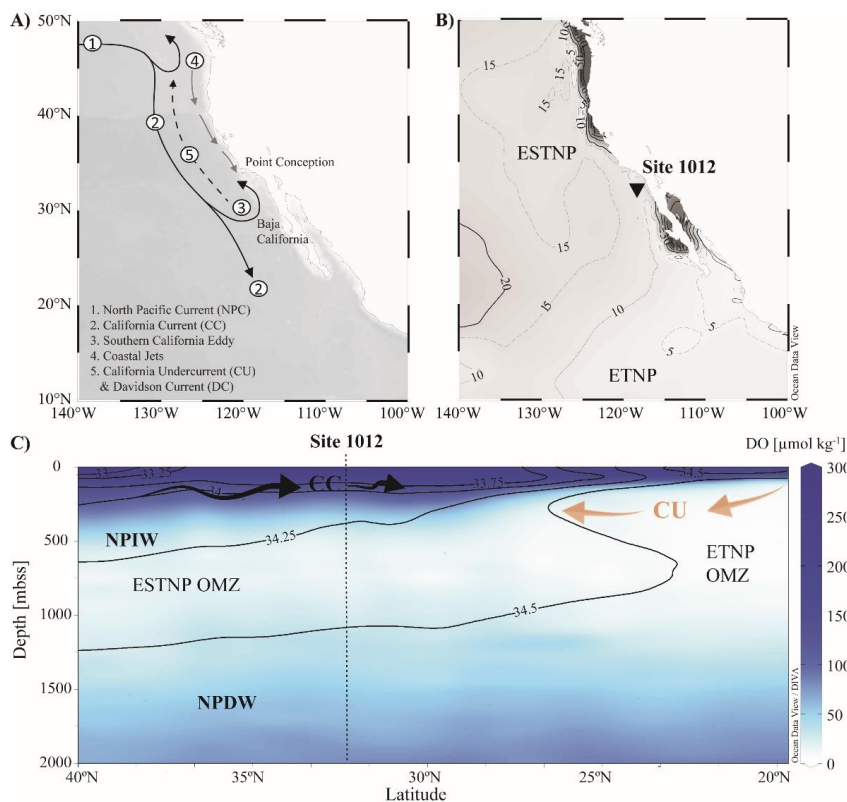
124 The sediment record was recovered in 1996 during Ocean Drilling Program (ODP) Leg 167 (Lyle et al., 1997) . Site 1012 is
125 located 105 km offshore California in the East Cortez Basin (32°16.970’N, 118°23.039’W), near the southern front of the
126 CC and northern front of the ETNP OMZ (Fig. 2B). The core was recovered from a water depth of 1784 m below sea surface
127 (mbss). For this study, 69 sediment depths (volumes of 20 cm^3) were selected for ladderane FAs analysis. Sedimentation
128 rates ranged from 4 to 15 cm kyr^{-1} (S1, Table 1). Considering the oldest detected ladderane FAs were in 140 ka BP
129 sediments (~10 m below sea floor ‘mbsf’) of the Arabian Sea (Jaeschke et al., 2009), we subsampled at a higher resolution
130 (every 10 to 50 cm) to the first ~160 kyr (15.7 mbsf) of the record (with a maximum resolution of 10 cm around T1 and T2)
131 and at a lower resolution (80 to 200 cm) to ~500 cal ka BP (37.5 mbsf). In addition, 74 sediments (10-50 cm resolution) were
132 analysed for bulk sedimentary organic carbon (TOC) and N (TN) content, and bulk isotopic ratio values ($\delta^{15}\text{N}$ and $\delta^{13}\text{C}$). A
133 detailed overview of all samples is given in Supplement 1, Tables 1 and 2. Samples were freeze-dried and stored at $-20 \text{ }^\circ\text{C}$
134 prior to analysis.

135 **3.2 Analysis of sedimentary bulk TOC, TN, $\delta^{13}\text{C}$ and $\delta^{15}\text{N}$**

136 Sediments were freeze-dried and ground to powder. For TOC and $\delta^{13}\text{C}$ analysis, aliquots of bulk sediment were decalcified
137 to remove all carbonates. Samples were first acidified with 2M hydrochloric acid (HCl) and rinsed with distilled water to
138 remove the salts. After the decalcification step, ca. 0.5 mg of dried material was used for the analysis. For TN and stable
139 nitrogen isotope ratio ($\delta^{15}\text{N}$) between 15 and 20 mg of non-decalcified sediment were used. All samples were packed in tin
140 cups and introduced to the Thermo Scientific Flash 2000 elemental analyzer coupled to a Thermo Scientific Delta V
141 Advantage isotope ratio mass spectrometer (EA/IRMS). Results are expressed in standard notation relative to Vienna Pee



142 Dece Belemnite (VPDB) for $\delta^{13}\text{C}$ and relative to air for $\delta^{15}\text{N}$. The precision as determined using laboratory standards
143 calibrated to certified international reference standards was in all cases $< 0.2\text{‰}$.



144

145 **Figure 2:** A) map of the California Current System (CCS). Key currents are indicated with arrows. B) location of ODP site 1012
146 ($32^{\circ}16.970\text{ N}$; $118^{\circ}23.039\text{ W}$) recovered at 1784 mbss, with minimum dissolved oxygen (DO) concentrations [$\mu\text{mol kg}^{-1}$] detected in the
147 water column in 2018 (WOA, 2018). C) A latitudinal section plot of the CCS water column showing modern annually averaged DO (μmol
148 kg^{-1}) concentrations and salinity (psu) concentrations with the color bar and contour lines, respectively (WOA, 2018). Major current and
149 water masses are also indicated, i.e., the Eastern Tropical and Eastern Subtropical North Pacific (ETNP and ESTNP, respectively) OMZs,
150 the California Current (CC; black arrows), the California Undercurrent (CU; orange arrows), North Pacific intermediate waters (NPIW)
151 and North Pacific deep water (NPDW). Maps were created in Ocean Data View and DIVA gridding was applied for interpolation of DO
152 concentrations (Schlitzer and Reiner, Ocean Data View, 2021).

153 3.3 Age model

154 Liu et al. (2005) previously constructed an age model for ODP site 1012, based on sediments recovered from Hole B. As the
155 material used in this study is predominantly from Hole A and C, a revised age model was constructed (S1, Table 1). The
156 revised age model for sediments up to 160 cal ka BP (15.7 m composite depth, 'mcd') was created by correlation of the bulk



157 sedimentary $\delta^{15}\text{N}$ record of Liu et al., (2005) with our dataset. Tie points (age vs composite depth) were selected by fine-
158 tuning using QAnalyseries (version 2022). For sediments >160 cal ka BP, which were solely sampled for ladderane FAs at
159 low resolution (i.e. not sedimentary $\delta^{15}\text{N}$), the age model of Liu et al. (2005) is used.

160 3.4 Ladderane extraction

161 Homogenized, freeze-dried sediments were extracted using a low temperature - low pressure accelerated solvent extraction
162 (ASE) method, previously described for ladderane extraction in Rush et al. (2012b). Thereafter, aliquots of the total lipid
163 extract were saponified in 2 N potassium hydroxide (in a 96 % MeOH solution) by refluxing for 1 h. After, 2 mL of
164 bidistilled water was added. The saponified extracts were acidified by adjusting the pH to 3 with 2 N hydrochloric acid (in a
165 50 % MeOH solution). Phase separation was induced by adding 2 mL of DCM. The biphasic mixtures were sonicated for 5
166 min and centrifuged for 2 min (3000 rpm). The DCM layers, containing the FAs, were collected. The mixtures were
167 partitioned twice more with DCM, after which the same procedure was applied before collection of the DCM layers. The FA
168 fractions were dried over a sodium sulphate (Na_2SO_4) column. Then, the fractions were methylated with diazomethane to
169 convert FAs into their corresponding fatty acid methyl esters (FAMES) and allowed to air-dry overnight to avoid losing the
170 more volatile SC-ladderane FA had they been dried under a stream of N_2 . The methyl esters of the polyunsaturated fatty
171 acids (PUFAs) were removed by eluting the FAME fractions with DCM over a silica impregnated silver nitrate (AgNO_3)
172 column. FAME fractions were dissolved in acetone and filtered over 0.45 mm PTFE filters (4 mm; BGB, USA).

173 3.5 Ladderane analysis

174 A commercially available deuterated $\text{C}_{20}[5]$ -PUFA (Reagecon Diagnostics Ltd.) was added as an internal standard to the
175 FAME fractions. FAME fractions were analysed on an Agilent 1290 Infinity I ultra-high performance liquid
176 chromatographer (UHPLC), equipped with a thermostatted auto-injector and column oven, coupled to a Q Exactive Plus
177 Orbitrap MS, with an atmospheric pressure chemical ionization (APCI) probe (Thermo Fischer Scientific, Waltham, MA)
178 operated in positive ion mode. Separation was achieved with a ZORBAX Eclipse XDB C_{18} column (Agilent, 3.0×250 mm,
179 5 μm), using MeOH as an eluant (0.4 ml min^{-1}). APCI source settings were set as follows: corona discharge current, 2.5 μA ;
180 source CID, 10 eV; vaporizer temperature, 475°C; sheath gas flow rate, 50 arbitrary units (AU); auxiliary gas flow rate,
181 30AU; capillary temperature, 300°C; and S-lens, 50V (van Kemenade et al., 2022). A mass range of m/z 225–380 was
182 monitored (resolution 140,000 ppm), followed by data-dependent MS^2 (resolution 17,500 ppm at m/z 200), in which the 10
183 most abundant masses in the mass spectrum were fragmented successively (stepped normalised collision energy 20, 25, 30).
184 An inclusion list containing the exact masses of C_{14-24} -[3]- and C_{14-24} -[5]-ladderane FAMES was used. Mass chromatograms
185 (within 5 ppm mass accuracy) of the protonated molecules ($[\text{M}+\text{H}]^+$) were used to integrate the detected ladderanes: $\text{C}_{14}[3]$ -,
186 $\text{C}_{14}[5]$, $\text{C}_{16}[5]$, $\text{C}_{18}[3]$ -, $\text{C}_{18}[5]$ -, $\text{C}_{20}[3]$ - and $\text{C}_{20}[5]$ -ladderane FAMES (m/z 235.169, 233.154, 261.185, 291.232, 289.216,



187 319.263 and 317.248, respectively), and the internal deuterated C₂₀[5]-PUFA standard (*m/z* 322.279). Identification of
188 ladderanes was achieved by comparing retention times and spectra with in-house isolated C₂₀[3]- and C₂₀[5]-ladderane
189 FAME standards (Hopmans et al., 2006; Rattray et al., 2008) and with ladderane FAMES in a biomass sample of *Ca.*
190 *Kueneria*.

191 Previously, ladderane FAME quantification has been conducted using calibration curves of in-house isolated C₂₀[3]-
192 and [5]-ladderane standard (Hopmans et al., 2006). However, this quantification method does not correct for any variability
193 in ion intensity, due to e.g., matrix effects and/or changes in the instruments functioning. Therefore, we further optimised
194 this quantification method to include a response correction using a commercially available internal standard (deuterated
195 C₂₀[5]-PUFA). At the start of each sequence, calibration curves were made for the C₂₀[3]- and [5]-ladderane standards *and*
196 the deuterated C₂₀[5]-PUFA standard. The relative response of the deuterated C₂₀[5]-PUFA commercial standard in relation
197 to the ladderane FAME standards was determined from the slopes of their calibration curves (giving a relative response
198 factor, i.e. RRF). An RRF of 1.3 was used for [3]-ladderanes, based on the C₂₀[3]-ladderane, and an RRF of 1.2 for the [5]-
199 ladderane, based on the C₂₀[5]-ladderane. Using the RRFs, ladderane FAME concentrations (*C_L*, expressed in µg · g dry
200 weight⁻¹) were calculated as follows:

$$201 \quad C_L = \frac{m_{IS} \left(\frac{A_L}{A_{IS}} \right)}{m_S} \quad [1]$$

202 With *m_{IS}* being the mass (µg) of the added internal standard, *m_S* the dry weigh of extracted sediment (g), *A_L* the integrated
203 peak area of the given ladderane FAME, *A_{IS}* the integrated peak area of the internal standard, and RRF the relative response
204 factor. Ladderane concentrations (including concentrations normalized against gram TOC) are reported in supplement 1
205 (Tables 4 and 5). To compare with previous studies that did not use an internal standard, the established method that uses
206 external calibration curves of three authentic standards (Hopmans et al., 2006; Rush et al., 2012b; Rattray et al., 2010) was
207 also performed (S1, Table 8b; S2.2).

208 3.6 NL₅ index

209 The index of ladderane lipids with five cyclobutane rings (NL₅) correlates with the temperature at which they were
210 synthesised. The NL₅ index is calculated according to the following equation:

$$211 \quad NL_5 = \frac{C_{20[5]ladderane\ FA}}{C_{18[5]ladderane\ FA} + C_{20[5]ladderane\ FA}} \quad [2]$$

212 The empirical fourth-order sigmoidal relationship between the NL₅ index and temperature is then described by:



213
$$NL_5 = 0.2 + \frac{0.7}{1 + e^{-\left(\frac{T-16.3}{1.5}\right)}} \quad [3]$$

214 with temperature (T) in °C (Rattray et al., 2010).

215 3.7 Degradation rates and constants

216 Ladderane degradation rates were calculated using the following equations for lipid degradation constants and rates (Canuel
217 and Martens, 1996):

218
$$k' = \frac{-\ln\left(\frac{C_t}{C_{t0}}\right)}{t} \quad [4]$$

219 With k' being the first order rate constant (kyr^{-1}), C being the concentration ($\mu\text{g g sediment}^{-1}$) at time t (C_t) and at the initial
220 time (C_{t0}), and t being the relative time (kyr).

221 4 Results

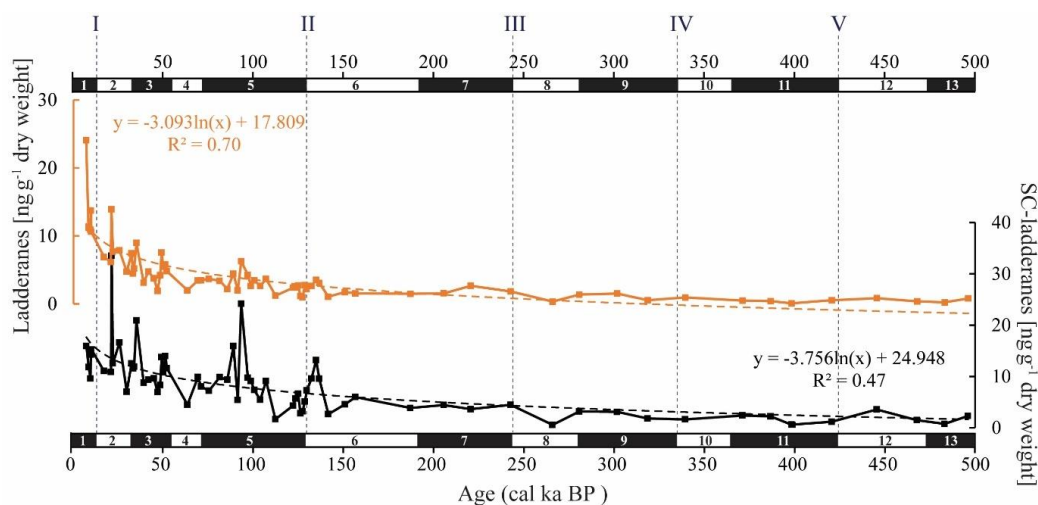
222 4.1 Bulk sedimentary total nitrogen and total organic carbon

223 Bulk sedimentary total nitrogen (TN) ranges between 0.1–0.6 % throughout the record. $\delta^{15}\text{N}$ fluctuates from 5.8 to 10.0 ‰.
224 An offset of 3 to 4 ‰ is observed between interglacials and glacials, with higher values during interglacials. The content of
225 sedimentary total organic carbon (TOC) varies between 1.7–7.4 % throughout the record, whilst its carbon isotopic
226 composition ($\delta^{13}\text{C}_{\text{TOC}}$) ranges from -23.0 to -21.6 ‰ (S1, Table 3).

227 4.2 Ladderane FAs

228 4.2.1 Ladderane FAs concentrations & the NL_5 index

229 The ladderane fatty acids identified in this record are $C_{18}[5]$ -, $C_{18}[3]$ -, $C_{20}[5]$ - and $C_{20}[3]$ -ladderanes and their diagenetic
230 products, the SC $C_{14}[5]$ -, $C_{14}[3]$ - and $C_{16}[5]$ -ladderanes. Normalized concentrations over the 160 ka record ranged as follows:
231 $C_{14}[5]$ -ladderane 16–158 ng gTOC⁻¹, $C_{14}[3]$ -ladderane 27–184 ng gTOC⁻¹, $C_{16}[5]$ -ladderane 34–198 ng gTOC⁻¹, $C_{18}[5]$ -
232 ladderane 7–107 ng gTOC⁻¹, $C_{18}[3]$ -ladderane 4–76 ng gTOC⁻¹, $C_{20}[5]$ -ladderane 5–79 ng gTOC⁻¹, and $C_{20}[3]$ -ladderane 10–
233 208 ng gTOC⁻¹ (S1, Table 4). Summed SC-ladderane and ladderane concentrations over the entire 500 ka record are 0.5–33
234 and 0.1–23 ng g⁻¹ dry weight, respectively (Fig. 3; S1 Table 5). Concentrations calculated without the use of the internal
235 standard (Hopmans et al., 2006; see section 2.5), are reported in S1 (Table 8b). The NL_5 index (eq. [2]) ranges from 0.3 to
236 0.8 throughout the record. Corresponding NL_5 -derived temperatures (eq. [3]) are between 13.1–18.6°C (S1, Table 6).



237

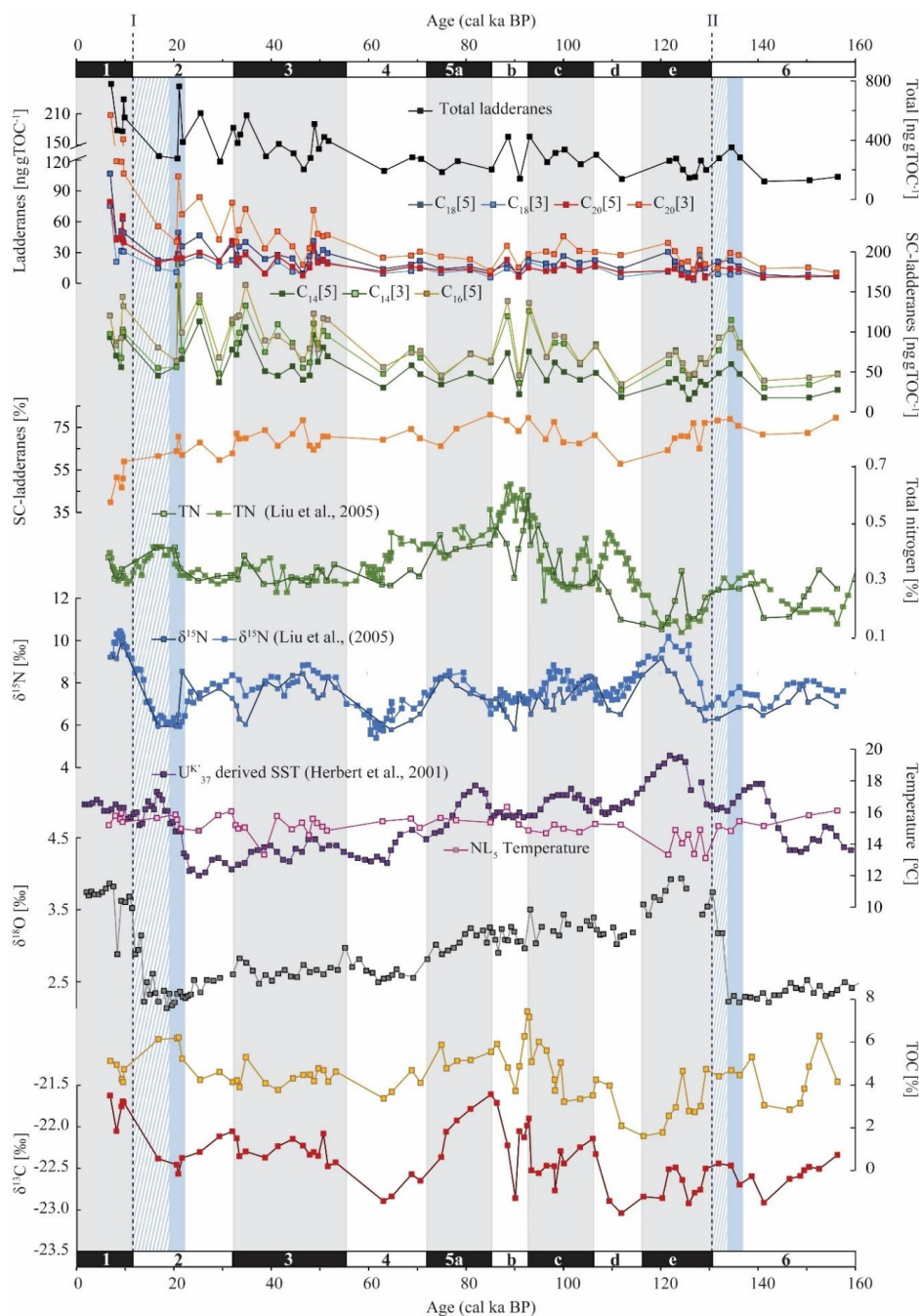
238 **Figure 3:** Summed C₁₈[5]-, C₁₈[3]-, C₂₀[5]- and C₂₀[3]-ladderane (orange) and summed short-chain (SC) C₁₄[5]-, C₁₄[3]- and C₁₆[5]-
239 ladderane (black) concentrations (ng g⁻¹ dry weight) in the ODP 1012 record. The logarithmic relationship between ladderanes and SC-
240 ladderanes with time is provided (with corresponding R²), and displayed with orange and black spaced lines, respectively. Grey spaced
241 lines indicate the approximate timing of glacial terminations I to V. N.B. the scales of the y-axes are different.

242 5 Discussion

243 In the sediment record of ODP site 1012, both short chain C₁₄[3]-, C₁₄[5]-, C₁₆[5]- as well as C₁₈[3]-, C₁₈[5]-, C₂₀[3]- and
244 C₂₀[5]- ladderane FAs were detected over the last 500 kyr (~38 mbsf; Fig. 3). This poses a considerable extension of the
245 ladderane record (formerly detected up to ~140 ka BP in Arabian Sea sediments; ~10 mbsf; Jaeschke et al., 2009). Below,
246 we will first discuss the provenance of the detected ladderane lipids (section 5.1). Then, their variability throughout glacial-
247 interglacial cycling (section 5.2), ending with the subsequent implications on our understanding of the nitrogen cycle of the
248 CCS (section 5.3). Unfortunately, the coarse sampling resolution in >160 cal ka BP sediments may have missed important
249 variations, and therefore, analysis of trends in ladderane concentrations over (inter)glacial cycling is limited to <160 cal ka
250 BP sediments.

251 5.1 Ladderanes sourced from anammox bacteria in the ESTNP OMZ water column

252 The relative contribution of SC-ladderanes to the total ladderane pool is a measure of oxygen exposure (Rush et al., 2011,
253 2012b), and the NL₅-index is a measure of the water temperature of the niche of anammox bacteria (Rattray et al., 2010). In
254 combination, these data may provide insights into the origin of ladderanes in the CCS sediment record.



255

256 **Figure 4:** From top to bottom: total ladderane (summed SC-ladderane and ladderane) normalized against TOC [ng gTOC⁻¹], ladderane and
 257 SC-ladderane accumulation rates [$\mu\text{g}^{-1}\text{cm}^{-2}\text{kyr}^{-1}$], relative abundance of SC-ladderanes over total ladderanes [%], total nitrogen (TN) from
 258 Liu et al., (2005) and this study [%], bulk sedimentary $\delta^{15}\text{N}$ from Liu et al., (2005) and this study [‰], U^{K}_{37} derived sea-surface
 259 temperatures (SST) from Herbert et al., (2001) and NL_5 -derived temperatures from this study [°C], benthic $\delta^{18}\text{O}$ record from Herbert et al.,
 260 (2001) [‰], total organic carbon (TOC) [%] and bulk sedimentary $\delta^{13}\text{C}$ [‰]. All data is derived from the same location (ODP site 1012).



261 Marine isotope stages (MIS) are indicated with black and white bars. Periods of maximum global ice volume (Herbert et al., 2001; blue
262 bars), deglaciation (striped blue bars) and the approximate timing of glacial terminations TI and TII (dashed lines) are also indicated.

263 In the CCS, a progressive depletion of both the water column $\delta^{15}\text{N}_{\text{NO}_3}$ and sedimentary $\delta^{15}\text{N}$ signal occurs with
264 increasing latitude, resulting in more depleted values at ODP site 1012 (8–10 ‰; Altabet et al., 1999; Liu et al., 2005; this
265 study) than in the ETNP OMZ core. The northward transport of denitrified waters by the poleward flowing oxygen-poor CU
266 from the core of the ETNP has been evoked to explain this trend (Castro et al., 2001; Kienast et al., 2002). However, a
267 similar mechanism is unlikely to explain the presence of ladderane FAs at ODP site 1012. Ladderane FAs are relatively
268 labile compounds, and in the Arabian Sea have been shown to already degrade into their SC-products (at relative proportions
269 of ~20 %) within the OMZ water column ($\text{DO} < 3 \mu\text{mol L}^{-1}$). There, the sinking of ladderanes through the oxygenated
270 bottom waters underlying the OMZ ultimately resulted in a relative abundance SC-ladderanes in the surface sediments of
271 20–80 %, depending on water column depth (Rush et al., 2012b).

272 At ODP site 1012, SC-ladderanes were present in similar relative abundances (40–88 %) throughout the record
273 (Fig. 4). The similarly high contribution of SC-ladderanes in the ODP 1012 record suggest ladderanes are also sourced from
274 an overlying OMZ water column (i.e. the ESTNP OMZ) and sunk through oxygenated bottom waters before being deposited
275 on the seafloor, which readily became anoxic in view of the high TOC content (Fig. 4). An OMZ water column source is
276 consistent with NL_5 -derived temperatures (13–17°C; S1, Table 6), which are significantly higher than what would be
277 expected for sedimentary anammox bacteria (i.e., modern annual average bottom water temperatures at site 1012 are <5°C;
278 WOA, 2018). And, while transport of ladderane FAs has been shown to occur within oxygen-depleted systems (van
279 Kemenade et al., 2022), long-distance transport of ladderane FAs with the CU (characteristic DO concentration of ~62 μmol
280 L^{-1} in modern CU water; Sahu et al., 2022) is unlikely, and would be expected to yield higher relative abundances of SC-
281 ladderane FAs than detected in the record. Transport of ladderanes is also not reflected in present-day ENP ladderane
282 distributions, as an investigation of ladderanes at a more northerly (~20°N) and a more southerly (~17°N) located site
283 showed *in situ* synthesis by pelagic *Ca. Scalindua* at both sites (Sollai et al., 2015). Hence, ladderane FAs are thought to
284 predominantly derive from the ESTNP OMZ water column and reflect a local anammox signal.

285 5.2 Anammox variability in the CCS over the last 160 kyr

286 5.2.1 The Holocene and MIS-5, including the penultimate interglacial of MIS 5e

287 Over the ~500 cal ka BP record, ladderane FAs are observed to decrease logarithmically with time (Fig. 3; $R^2 = 0.70$), in
288 which the degradation constant k follows a linear relationship (when logarithmically transformed; Fig. 5A; $R^2 = 0.88$) with
289 time. This is consistent with first order degradation kinetics, typical for OM (Canuel and Martens, 1996). As such, it is not
290 surprising that the highest ladderane concentrations are observed in the youngest sediments, deposited during the early to



291 mid-Holocene. Even so, ladderane FAs normalized against TOC also show elevated concentrations in Holocene sediments.
292 This suggests high ladderane FAs at this time are not simply a preservation signal but also reflect an increase (compared to
293 pre-Holocene sediments) in their production by *Ca. Scalindua* spp. relative to the total organic C pool. Moreover, elevated
294 ladderanes in early to mid-Holocene sediments coincide with enriched bulk $\delta^{15}\text{N}$ (9–10 ‰), indicative of increased N-loss by
295 anaerobic microorganisms, and TOC and TN concentrations (Fig. 4), indicative of increased productivity.

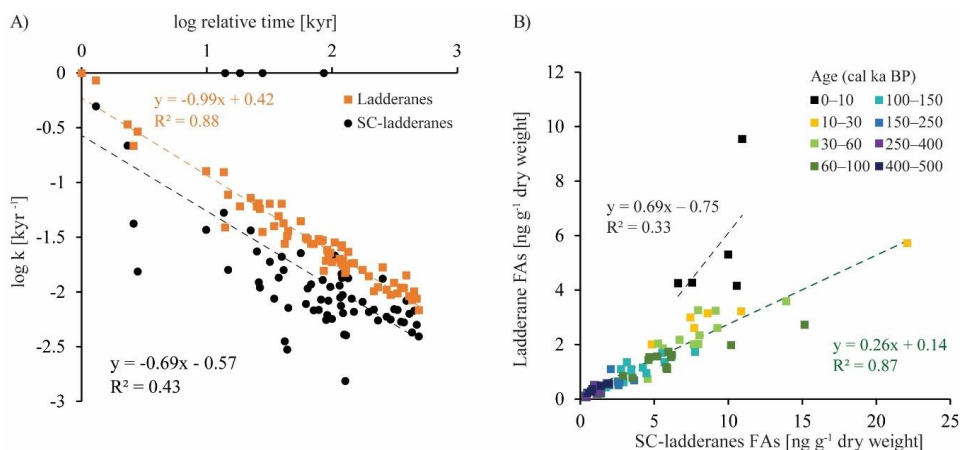
296 Interestingly, SC-ladderane FA concentrations are not highest in Holocene sediments. Consequently, the
297 SC-ladderane data does not fit the logarithmic decrease with time well ($R^2 = 0.34$; Fig. X), which is also reflected in the
298 relationship of the degradation constant k with time (Fig. 5A; $R^2 = 0.43$). The oxidation of ladderane FAs to produce SC-
299 ladderane FAs (Rush et al., 2011) has been shown to take place within the oxic waters below the OMZ. In this way, 20–80 %
300 of the ladderane FAs were transformed into SC-ladderanes in the Arabian Sea (Rush et al., 2012c). Throughout the deeper
301 CCS sedimentary record (>10 cal ka BP), the relationship between ladderane FAs and their SC-products follows a linear
302 trend ($R^2 = 0.88$; Fig. 5B), with SC-ladderanes making ~60–80 % of total ladderanes (Fig. 4). However, in Holocene
303 sediments (<10 cal ka BP sediments), the relationship between ladderanes and SC-ladderanes is different (Fig. 5B), and SC-
304 ladderanes occur at relatively lower abundance (40–60 % in Fig. 4) compared to the rest of the record. This appears to
305 indicate that after 10 cal ka BP, there was no significant change in the exposure of ladderane FAs to the oxygenated water
306 underlying the ETNP OMZ before being buried in the sediment record, but that in the recent record, there was reduced
307 oxygen exposure.

308 Lembke-Jene et al. (2018) showed, using palaeoceanographic proxies and palaeomodelling, that a combination of
309 sea ice loss, increased SST and remineralization rates led to more deoxygenated intermediate waters (the NPIW) during the
310 early to mid-Holocene in the North Pacific. Moreover, in the ETNP, enriched sedimentary $\delta^{15}\text{N}$ values and laminated
311 sediments during the early Holocene, alongside geochemical tracers, have been interpreted to signal the presence of a strong
312 OMZ at this time, while bioturbated sediments occurred over the last glacial period (Thunell and Kepple, 2004).

313 Ladderane FAs concentrations also peak during the penultimate interglacial (the Eemian; MIS 5e), in line with
314 enriched (>8 ‰) $\delta^{15}\text{N}$ values. Microfossil data from MIS 5 has indicated that intermediate waters in the western North
315 Pacific were more deoxygenated during the Eemian (Matul et al., 2016), which may have driven increased anammox in the
316 CCS at this time. However, ladderane FAs concentrations during mid-MIS 5 (MIS 5b–c; Fig. 4) are even more elevated,
317 while the $\delta^{15}\text{N}$ signal here is subdued (<8 ‰). Ladderane trends in MIS 5 hereby seem to follow paleo-productivity proxies
318 (i.e., TOC and TN) more closely (which also peak during MIS 5b–c; Fig. 4). During MIS 5b–d, intermediate waters in the
319 western North Pacific were oxic (Matul et al., 2016). Indeed, over the course of MIS 5, from late MIS 5e onwards, SSTs in
320 the CCS decreased while the CC strengthened (Herbert et al., 2001; Yamamoto et al., 2007). This would have led to



321 increased transport of high-oxygen, nutrient-rich NPIW (Herguera et al., 2010) and enhanced open ocean upwelling. At the
322 same time, this would have fuelled productivity, which is reflected in the high TOC and TN concentrations in mid-MIS 5.



323
324 **Figure 5:** A) Linear relationship between the logarithmic values of the degradation constant k and relative time for ladderane FAs (orange
325 squares) and SC-ladderane FAs (black dots). B) Relationship between ladderane FAs and SC-ladderane FAs, in which samples are colour-
326 coded according to age. The linear relationship and corresponding R^2 are given for the most recent age group (0-10 cal ka BP; in black)
327 and the >10 cal ka BP age groups (in green).

328 Babbin et al., (2014) showed, using incubations from the ETNP OMZ, that anammox rates increase in response to
329 the addition of OM. Likewise, in the modern Southern Pacific OMZ, N-loss by anammox was found to be strongly
330 correlated with the export of OM, via the release of ammonium into the water column through remineralization (Kalvelage et
331 al., 2013). As such, the co-variation of ladderane FAs with paleo-productivity proxies, could reflect an increase in *Ca.*
332 *Scalindua* spp. abundance in response to an increased N-substrate supply via OM-remineralization or nutrient transport,
333 rather than a response to changing DO concentration. Even so, the increased OM-supply during MIS 5b-d could also have
334 led to more reducing conditions via OM-remineralization within the ENP OMZ, which may not be recorded in the western
335 part of the North Pacific. The discrepancies between the ladderane- and $\delta^{15}\text{N}$ record at this time, and consequent implications
336 for our understanding of the N-cycle in the CCS are further discussed in section 5.3.

337 5.2.2 The two most recent glacial periods

338 Ladderane FAs are observed to increase from early MIS 3 to mid-MIS 2, and from mid- to late-MIS 6. Maxima of
339 ladderanes occur approximately at the timing of icesheet volume maxima of the last glacial maxima (LGM) and the
340 penultimate glacial of MIS 6 (blue bars in Fig. 4; following timing of Herbert et al., 2001). During the last glacial period
341 (~115–12 ka BP) and the penultimate glacial MIS 6, large parts of the North American continent were covered by the
342 Laurentide and Cordilleran ice sheets. While glacials are typically associated with a well-ventilated intermediate-water mass



343 (Herguera et al., 2010) and a strong southward advection of the CC (Ortiz et al., 1997), a weakening of the CC has been
344 proposed to occur at times of global ice sheet maxima. In the CCS, $U^{K'_{37}}$ -derived temperatures indicate that SSTs increased
345 ~12 kyr in advance of maximal ice-sheet volumes. This is thought to reflect increased northward advection of warm oxygen-
346 poor waters carried by the CU and DC in response to a weakened CC due to large ice-sheet volumes (Herbert et al., 2001).
347 Using trace elements, Cartapanis et al., (2011) found that intermediate water oxygenation off Baja California deteriorated
348 slightly over the course of late MIS 3 and early MIS 2, consistent with a strengthening of the CU at this time. As such, the
349 increased abundance of ladderanes observed during (and leading up to) ice sheet maxima at ODP site 1012, may derive from
350 an increased *Ca. Scalindua* spp. abundance due to more reduced local conditions, via the enhanced strength of the CU.

351 In contrast, low ladderane concentrations occur at times of deglaciation (T1: ~19–11 ka BP and T2: ~135–128 ka
352 BP). Modelling-studies have proposed that during the early part of the Last Glacial Termination (~17.5–15.0 ka BP), a
353 reorganization of the global conveyor belt circulation would have led to deep water formation in the North Pacific, extending
354 to ~2500 to 3000 mbss. In turn, this would have led to nutrient-poor but well-ventilated intermediate-deep waters (Okazaki
355 et al., 2010; Menviel et al., 2011). At the same time, there was increased influx of freshwater from the Cordilleran ice-sheet
356 into the northeastern Pacific. Increased melt-water influx during deglaciation would have strengthened the southward forcing
357 of the oxygen-rich CC, and consequently weakened the CU (Herbert et al., 2001). As such, increased ventilation of glacial
358 NPIW and decreased northward forcing of the CU may have reduced the extension of the anoxic ESTNP core available for
359 anammox, which may explain the observed ladderane minima during deglaciation. Ladderane and $\delta^{15}\text{N}$ minima (~5.9 ‰
360 during T1 and ~6.8 ‰ during T2) coincide, suggesting limited loss of bioavailable N via anammox and denitrification at this
361 time. In contrast, in the Gulf of Tehuantepec Thunell and Keppel (2004) recorded increasing $\delta^{15}\text{N}$ values over 23–17 ka, with
362 maximum values during the Bølling–Allerød warming period. Differences between the $\delta^{15}\text{N}$ records between this (~15‰)
363 and more northerly located sites (e.g., ODP site 1012) over T1, has been explained by the presence of a hydrographic
364 boundary within the ETNP around ~20°N at this time, which kept northern- and southern-sourced intermediate waters
365 separate (Hendy and Pedersen, 2006).

366 **5.3 Implications of the occurrence of anammox on the N cycle in the CCS**

367 In the CCS, previous estimates of changes in N-loss over time have been based on the bulk sedimentary $\delta^{15}\text{N}$ record.
368 Enriched $\delta^{15}\text{N}$ during interglacials (7–10 ‰) are thought to reflect intensified denitrification in response to reduced DO,
369 while more depleted $\delta^{15}\text{N}$ during glacial (4–6 ‰) are assumed to reflect lowered rates in response to increased DO (Liu et
370 al., 2005; 2008). However, the high abundance of ladderane FAs throughout our CCS record (i.e. up to a factor ~5 higher
371 than in the Arabian Sea record; Jaeschke et al., 2009) now shows that anammox was (also) responsible for N-loss and thus
372 contributed, at least partially, to the sedimentary $\delta^{15}\text{N}$ record.



373 The correlation of the $\delta^{15}\text{N}$ record with SST reconstructions (Liu et al., 2005) shows that fluctuations in $\delta^{15}\text{N}$ occur
374 in tandem with glacial-interglacial cycling. However, a long-standing conundrum has been the discrepancy between the $\delta^{15}\text{N}$
375 record and productivity proxies (i.e., TOC and TN), especially north of the ETNP (Kienast et al., 2002), as also seen in our
376 record (Fig. 4). This decoupling has been used previously to suggest that variations in denitrification was not due to changes
377 in OM remineralization rate, but rather from changes in ocean circulation and ventilation patterns (Ganeshram et al., 2000).
378 Yet, fluctuations in ladderanes *do* seem to follow trends in paleo-productivity proxies (i.e., TOC and TN) relatively closely,
379 especially during the Holocene, MIS 3 and MIS 5. And, while enriched $\delta^{15}\text{N}$ values sometimes correspond to ladderane
380 maxima (i.e. during the Holocene), discrepancies with ladderane concentrations are seen especially during MIS 3 and MIS 5,
381 and during glacial periods (Fig. 4).

382 Out-of-phase anammox and denitrification could be caused by variations in the C:N ratio of OM. Given the average
383 C:N signature of marine OM (106:16; Redfield, 1963), stoichiometric constraints should result in a ratio of N_2 production via
384 denitrification and anammox of 71:29 (Koeve and Kähler, 2010). Localized variations in the C:N signature may result in
385 different relative contributions. Yet, integrating these variations over space and time should obtain a similar ratio (Dalsgaard
386 et al., 2012; Ward, 2013; Babbín et al., 2014). As such, given the temporal resolution of the record (which does not cover
387 seasonality), denitrification and anammox intensities are expected to fluctuate in-tandem.

388 Moreover, both denitrifiers and anammox bacteria are similarly inhibited by oxygen in the marine environment, at
389 DO concentration above 3 to 8 $\mu\text{mol L}^{-1}$ (Babbín et al., 2014). Furthermore, Babbín et al., (2014) showed, using incubations
390 from the ETNP OMZ, that both denitrification and anammox are limited by OM supply, and their rates increase in response
391 to the addition of OM. As anammox bacteria are autotrophic, this may be explained by the dependence of the process on
392 NH_4^+ and NO_2^- availability, which can a.o. be supplied via remineralization. As such, both anammox and denitrification
393 should respond similarly to changes in DO and OM in the CCS.

394 Reconstructions of N-loss using sedimentary $\delta^{15}\text{N}$ depend on the assumption that there was complete biological
395 utilization of NO_3^- by phytoplankton. However, during periods of high upwelling intensity (as likely occurred during mid-
396 MIS 5; see section 5.2.1), the high NO_3^- availability may result in incomplete NO_3^- assimilation. This allows for the
397 preferential uptake of ^{14}N by primary producers, resulting in a pool of $\delta^{15}\text{N}$ depleted OM available for heterotrophic
398 denitrification (Tesdal et al., 2013). Hence, at times of high NO_3^- supply, incomplete nitrate assimilation would have
399 quenched the $\delta^{15}\text{N}$ signal, even if denitrification was as intense as during periods of low NO_3^- availability. Moreover, a study
400 by Altabet and Francois (1994) showed that sedimentary $\delta^{15}\text{N}$ in the equatorial Pacific records the isotopic enrichment of
401 near-surface NO_3^- via depletion by phytoplankton, in which enriched $\delta^{15}\text{N}$ values are associated with reduced NO_3^-
402 availability for phytoplankton assimilation. Also, in the South Pacific, NO_3^- concentrations have been found to affect the U
403 $^{K_r}_{37}$ index (Placencia et al., 2010). Given the excellent correlation between the $\delta^{15}\text{N}$ and $U^{K_r}_{37}$ -based SST records of the CCS



404 (Liu et al., 2005) and the discrepancies between the $\delta^{15}\text{N}$ and ladderane records, it may be sensible to conclude that the CCS
405 sedimentary $\delta^{15}\text{N}$ fluctuations (also) record variations in NO_3^- assimilation by phytoplankton.

406 Additionally, other biological processes may influence the $\delta^{15}\text{N}$ signal (Zonneveld et al., 2010). In the Gulf of
407 Tehuantepec, at the southern end of the ETNP OMZ core, $\delta^{15}\text{N}$ values decrease over the course of the Holocene (Thunell and
408 Kepple, 2004; Hendy and Pedersen, 2006), while laminated sediments suggest reduced DO concentrations. This was
409 interpreted as being the result of increased N_2 -fixation ($\epsilon: \leq +2\%$; Sigman and Fripiat, 2019), which lowered the
410 “denitrification” $\delta^{15}\text{N}$ signal (Thunell and Kepple, 2004). Lastly, enrichment of the sedimentary $\delta^{15}\text{N}$ values occurs during
411 early burial, where oxygen exposure results in enhanced biological isotopic alteration (Robinson et al., 2012). In short,
412 sedimentary $\delta^{15}\text{N}$ is shaped by many opposing processes, and assuming a one-on-one relationship with denitrification
413 intensities and DO concentration clearly misses the complexity that shape the CC system. Ladderanes hereby offer a more
414 detailed picture of N-loss dynamics in the paleoenvironment of the CCS. In the case of the ODP site 1012 record, ladderane
415 concentration trends challenge the conventional assumption that N-loss processes solely follow ocean circulation and
416 ventilation patterns coupled to (inter)glacial cycling, and instead show OM remineralization may also be an important driver
417 of N-loss.

418 Discrepancies between the ladderane and $\delta^{15}\text{N}$ -record hereby necessitate careful consideration when applying N-
419 isotope based budgets to estimate past N-cycling. More specifically, the occurrence of increased ladderane concentrations
420 during glacial maxima may require a re-evaluation on the response of N-loss rates to glacial-interglacial cycling in the CCS.
421 Furthermore, the occurrence of an additional N-loss pathway in the CCS (anammox), other than denitrification, may affect
422 estimates of N_2O greenhouse-gas production by denitrifiers and the degree of heterotrophy of the system, although the
423 importance of this would require further investigation. Future research, investigating anammox biomarkers in other CCS
424 records (preferably in a latitudinal gradient with this record) may offer further insights into N-loss dynamics across glacial-
425 interglacial cycles.

426 **6 Conclusion**

427 Ladderane FAs detected in a ~500 kyr CCS sedimentary record at ODP site 1012 reveal the past occurrence of anaerobic
428 ammonium oxidising (anammox) bacteria in the water column of the California current system (CCS) over the last five
429 glacial terminations. The index of ladderanes with five cyclobutene moieties (NL_5), which correlates with the *in situ*
430 temperature at which ladderanes are synthesised, suggests that ladderanes were derived from the ETNP OMZ water
431 column. The high-resolution record of the last two interglacial-glacial transitions shows a continuous presence of ladderane
432 FAs, with maxima during: i) the Holocene, ii) leading up to and during the LGM (early MIS 3 to mid-MIS 2), iii) MIS 5b-c
433 and iv) during the ice sheet maxima of the penultimate glacial (late MIS 6). Combining information on the presence of



434 ladderanes with paleo-productivity proxies and the hydrographic features of the CCS suggests anammox abundance was
435 driven both by OM-remineralization and advection changes, which regulated nutrient and oxygen concentrations. In the
436 record, a clear shift is seen in the relationship of SC-ladderanes over their parent products, in which the relative abundance of
437 SC-ladderanes is significantly lower in Holocene than in pre-Holocene sediments. This may reflect a shift in oxygen
438 exposure, which corresponds to previous studies showcasing a vertical expansion of the ENP OMZ over the Holocene.
439 Clearly, the anammox contribution to N-loss in the CCS, as shown in this study, requires a reassessment of biogeochemical
440 cycling in this system. Discrepancies between the ladderane and $\delta^{15}\text{N}$ record may imply that N-loss was perhaps more
441 intense during cold phases than previously assumed. Careful considerations must thus be taken when using N-isotope based
442 budgets to estimate past N-cycling in the CCS; sedimentary $\delta^{15}\text{N}$ is shaped by many opposing processes, and assuming a
443 one-to-one relationship between N-loss intensities and OMZ variability clearly overlooks the complexity that shapes the CC
444 system. Ladderanes hereby offer a more holistic picture of N-loss dynamics in the paleoenvironment of the CCS.

445 **Data availability.** All data discussed in this paper is available in the supplementary material 1. Data from supplementary
446 material 1 can be retrieved via the following doi: 10.25850/nioz/7b.b.sg

447 **Supplement.** The supplement related to this article is available on-line at:

448 **Author contributions.** ZE and ZRvK performed the laboratory work. ZRvK conducted the data analysis and writing of the
449 manuscript. ZE created the age-model. ECH developed and optimized the UHPLC-HRMS method for the analysis of
450 ladderane lipids. DR provided the supervision of the project. DR, ZE and ZRvK designed and conceptualized the project.
451 JSSD provided critical support in data interpretation. All authors contributed to the writing of the manuscript.

452 **Competing interests.** The authors declare that they have no conflict of interest.

453 **Acknowledgements.** We thank the captain and crew of Ocean Drilling Program Leg 167 for the collection of all sampled
454 material used in this study. Denise Dorhout and Monique Verweij are also greatly appreciated for their support with the
455 instrumental analysis. We also kindly thank Ronald van Bommel and Marcel van der Meer for their help in the isotope lab.

456 **Financial support.** This research was supported by the Soehngen Institute of Anaerobic Microbiology (SIAM) Gravitation
457 Grant (024.002.002), awarded to JSSD by the Dutch Ministry of Education, Culture and Science (OCW).

458 **References.**

459 Altabet, M. A. and Francois, R.: Sedimentary nitrogen isotopic ratio as a recorder for surface ocean nitrate utilization, *Global*
460 *Biogeochem Cycles*, 8, 103–116, <https://doi.org/10.1029/93GB03396>, 1994.



- 461 Altabet, M. A., Pilskaln, C., Thunell, R., Pride, C., Sigman, D., Chavez, F., and Francois, R.: The nitrogen isotope
462 biogeochemistry of sinking particles from the margin of the eastern North Pacific, *Deep Sea Res 1 Oceanogr Res Pap*, 46,
463 655–679, [https://doi.org/10.1016/S0967-0637\(98\)00084-3](https://doi.org/10.1016/S0967-0637(98)00084-3), 1999.
- 464 Babbin, A. R., Babbin, A. R., Keil, R. G., Devol, A. H., and Ward, B. B.: Oxygen Control Nitrogen Loss in the Ocean, 406,
465 <https://doi.org/10.1126/science.1248364>, 2014.
- 466 Bakun, A. and Nelson, C. S.: The seasonal cycle of wind-stress curl in subtropical eastern boundary current regions, *J.*
467 *Physical Oceanography*, 21, 1815–1834, [https://doi.org/10.1175/1520-0485\(1991\)021<1815:TSCOWS>2.0.CO;2](https://doi.org/10.1175/1520-0485(1991)021<1815:TSCOWS>2.0.CO;2), 1991.
- 468 Bograd, S. J., Castro, C. G., di Lorenzo, E., Palacios, D. M., Bailey, H., Gilly, W., and Chavez, F. P.: Oxygen declines and
469 the shoaling of the hypoxic boundary in the California Current, *Geophys Res Lett*, 35, 1–6,
470 <https://doi.org/10.1029/2008GL034185>, 2008.
- 471 Bograd, S. J., Schroeder, I., Sarkar, N., Qiu, X., Sydeman, W. J., and Schwing, F. B.: Phenology of coastal upwelling in the
472 California Current, *Geophys Res Lett*, 36, 1–5, <https://doi.org/10.1029/2008GL035933>, 2009.
- 473 Canuel, E. A. and Martens, C. S.: Reactivity of recently deposited organic matter : near the sediment-water Degradation
474 interface of lipid compounds, 60, 1793–1806, 1996.
- 475 Cartapanis, O., Tachikawa, K., and Bard, E.: Northeastern Pacific oxygen minimum zone variability over the past 70 kyr :
476 Impact of biological production and oceanic ventilation, 26, 1–17, <https://doi.org/10.1029/2011PA002126>, 2011.
- 477 Castro, C. G., Chavez, F. P., and Collins, C. A.: Role of the California undercurrent in the export of denitrified waters from
478 the eastern tropical North Pacific, *Global Biogeochem Cycles*, 15, 819–830, <https://doi.org/10.1029/2000GB001324>, 2001.
- 479 Chavez, F. P. and Messié, M.: A comparison of Eastern Boundary Upwelling Ecosystems, *Prog Oceanogr*, 83, 80–96,
480 <https://doi.org/10.1016/j.pocean.2009.07.032>, 2009.
- 481 Checkley, D. M. and Barth, J. A.: Patterns and processes in the California Current System, *Prog Oceanogr*, 83, 49–64,
482 <https://doi.org/10.1016/j.pocean.2009.07.028>, 2009.
- 483 Choumiline, K., Pérez-Cruz, L., Gray, A. B., Bates, S. M., and Lyons, T. W.: Scenarios of Deoxygenation of the Eastern
484 Tropical North Pacific During the Past Millennium as a Window Into the Future of Oxygen Minimum Zones, *Front Earth Sci*
485 (Lausanne), 7, 1–23, <https://doi.org/10.3389/feart.2019.00237>, 2019.



- 486 Codispoti, L. A., Brandes, J. A., Christensen, J. P., Devol, A. H., Naqvi, S. W. A., Paerl, H. W., and Yoshinari, T.: The
487 oceanic fixed nitrogen and nitrous oxide budgets: Moving targets as we enter the anthropocene?, *Sci Mar*, 65, 85–105,
488 <https://doi.org/10.3989/scimar.2001.65s285>, 2001.
- 489 Dalsgaard, T., Thamdrup, B., Farías, L., and Revsbech, N. P.: Anammox and denitrification in the oxygen minimum zone of
490 the eastern South Pacific, *Limnol Oceanogr*, 57, 1331–1346, <https://doi.org/10.4319/lo.2012.57.5.1331>, 2012.
- 491 Dorman, C. E. and Winanat, C. D.: Buoy observations of the atmosphere along the west coast of the United States, 1981-
492 1990, *J Geophys Res*, 100, 1981–1990, <https://doi.org/10.1029/95jc00964>, 1995.
- 493 Fine, R. A., Maillet, K. A., Sullivan, K. F., and Willey, D.: Circulation and Ventilation flux of the Pacific Ocean, *J Geophys*
494 *Res Oceans*, 106, 22159–22178, <https://doi.org/10.1029/1999jc000184>, 2001.
- 495 Fu, W., Bardin, A., and Primeau, F.: Tracing ventilation source of tropical pacific oxygen minimum zones with an adjoint
496 global ocean transport model, *Deep Sea Res 1 Oceanogr Res Pap*, 139, 95–103, <https://doi.org/10.1016/j.dsr.2018.07.017>,
497 2018.
- 498 Galán, A., Molina, V., Thamdrup, B., Woebken, D., Lavik, G., Kuypers, M. M. M., and Ulloa, O.: Anammox bacteria and
499 the anaerobic oxidation of ammonium in the oxygen minimum zone off northern Chile, *Deep Sea Res 2 Top Stud Oceanogr*,
500 56, 1021–1031, <https://doi.org/10.1016/j.dsr2.2008.09.016>, 2009.
- 501 van de Graaf, A. A., Mulder, A., de Bruijn, P., Jetten, M. S. M., Robertson, L. A., and Kuenen, J. G.: Anaerobic oxidation of
502 ammonium is a biologically mediated process, *Appl Environ Microbiol*, 61, 1246–1251,
503 <https://doi.org/10.1128/aem.61.4.1246-1251.1995>, 1995.
- 504 van de Graaf, A. A., de Bruijn, P., Robertson, L. A., Jetten, M. S. M., and Kuenen, J. G.: Metabolic pathway of anaerobic
505 ammonium oxidation on the basis of ¹⁵N studies in a fluidized bed reactor, *Microbiology (N Y)*, 143, 2415–2421,
506 <https://doi.org/10.1099/00221287-143-7-2415>, 1997.
- 507 Gruber, N.: The Ocean Carbon Cycle and Climate, in: *The Ocean Carbon Cycle and Climate*, edited by: Follows, M. and
508 Oguz, T., Dordrecht, <https://doi.org/10.1007/978-1-4020-2087-2>, 2004.
- 509 Hamasaki, K., Shishikura, R., Suzuki, S., Shiozaki, T., Ogawa, H., Nakamura, T., and Suwa, Y.: Distribution and phylogeny
510 of anaerobic ammonium-oxidizing (anammox) bacteria in the water column of the central Pacific Ocean, *Deep Sea Res 2*
511 *Top Stud Oceanogr*, 156, 60–67, <https://doi.org/10.1016/j.dsr2.2017.11.013>, 2018.



- 512 Hamersley, M. R., Lavik, G., Woebken, D., Rattray, J. E., Lam, P., Hopmans, E. C., Sinninghe Damsté, J. S., Krüger, S.,
513 Graco, M., Gutiérrez, D., and Kuypers, M. M. M.: Anaerobic ammonium oxidation in the Peruvian oxygen minimum zone,
514 *Limnol Oceanogr*, 52, 923–933, <https://doi.org/10.4319/lo.2007.52.3.0923>, 2007.
- 515 Hendy, I. L. and Kennett, J. P.: Tropical forcing of North Pacific intermediate water distribution during Late Quaternary
516 rapid climate change?, *Quat Sci Rev*, 22, 673–689, [https://doi.org/10.1016/S0277-3791\(02\)00186-5](https://doi.org/10.1016/S0277-3791(02)00186-5), 2003.
- 517 Hendy, I. L. and Pedersen, T. F.: Oxygen minimum zone expansion in the Eastern Tropical North Pacific during
518 deglaciation, *Geophys Res Lett*, 33, 1–5, <https://doi.org/10.1029/2006GL025975>, 2006.
- 519 Herbert, T. D., Schuffert, J. D., Andreasen, D., Heusser, L., Lyle, M., Mix, A., Ravelo, A. C., Stott, L. D., and Herguera, J.
520 C.: Collapse of the California current during glacial maxima linked to climate change on land, *Science* (1979), 293, 71–76,
521 <https://doi.org/10.1126/science.1059209>, 2001.
- 522 Herguera, J. C., Herbert, T., Kashgarian, M., and Charles, C.: Intermediate and deep water mass distribution in the Pacific
523 during the Last Glacial Maximum inferred from oxygen and carbon stable isotopes, *Quat Sci Rev*, 29, 1228–1245,
524 <https://doi.org/10.1016/j.quascirev.2010.02.009>, 2010.
- 525 Hopmans, E. C., Kienhuis, M. V. V., Rattray, J. E., Jaeschke, A., Schouten, S., and Sinninghe Damsté, J. S.: Improved
526 analysis of ladderane lipids in biomass and sediments using high-performance liquid chromatography/atmospheric pressure
527 chemical ionization tandem mass spectrometry, *Rapid Communications in Mass Spectrometry*, 20, 2099–2103,
528 <https://doi.org/10.1002/rcm>, 2006.
- 529 Huyer, A.: Coastal upwelling in the California current system, *Prog Oceanogr*, 12, 259–284, <https://doi.org/10.1016/0079->
530 [6611\(83\)90010-1](https://doi.org/10.1016/0079-6611(83)90010-1), 1983.
- 531 Jaeschke, A., Ziegler, M., Hopmans, E. C., Reichert, G. J., Lourens, L. J., and Schouten, S.: Molecular fossil evidence for
532 anaerobic ammonium oxidation in the Arabian Sea over the last glacial cycle, *Paleoceanography*, 24,
533 <https://doi.org/10.1029/2008PA001712>, 2009.
- 534 Kalvelage, T., Lavik, G., Lam, P., Contreras, S., Arteaga, L., Löscher, C. R., Oshlies, A., Paulmier, A., Stramma, L., and
535 Kuypers, M. M. M.: Nitrogen cycling driven by organic matter export in the South Pacific oxygen minimum zone, *Nat*
536 *Geosci*, 6, 228–234, <https://doi.org/10.1038/ngeo1739>, 2013.
- 537 Van Kemenade, Z. R., Villanueva, L., Hopmans, E. C., Kraal, P., Witte, H. J., Sinninghe Damsté, J. S., and Rush, D.:
538 Bacteriohopanetetrol-x: Constraining its application as a lipid biomarker for marine anammox using the water column



- 539 oxygen gradient of the Benguela upwelling system, *Biogeosciences*, 19, 201–221, <https://doi.org/10.5194/bg-19-201-2022>,
540 2022.
- 541 van Kemenade, Z. R., Cutmore, A., Hennekam, R., Hopmans, E. C., van der Meer, M. T. J., Mojtahid, M., Jorissen, F. J.,
542 Bale, N. J., Reichart, G. J., Sinninghe Damsté, J. S., and Rush, D.: Marine nitrogen cycling dynamics under altering redox
543 conditions: Insights from deposition of sapropels S1 and the ambiguous S2 in the Eastern Mediterranean Sea, *Geochim
544 Cosmochim Acta*, 354, 197–210, <https://doi.org/10.1016/j.gca.2023.06.018>, 2023.
- 545 Kemp, A. E. S., Langhorne, D. N., Fairchild, I. J., Schmitt, T. S., and Nisbet, E. G.: Evidence for abrupt climate changes in
546 annually laminated marine sediments, *Philosophical Transactions of the Royal Society A: Mathematical, Physical and
547 Engineering Sciences*, 361, 1851–1870, <https://doi.org/10.1098/rsta.2003.1247>, 2003.
- 548 Kienast, S. S., Calvert, S. E., and Pedersen, T. F.: Nitrogen isotope and productivity variations along the northeast Pacific
549 margin over the last 120 kyr: Surface and subsurface paleoceanography, *Paleoceanography*, 17, 7-1-7–17,
550 <https://doi.org/10.1029/2001PA000650>, 2002.
- 551 Kobayashi, K., Makabe, A., Yano, M., Oshiki, M., Kindaichi, T., Casciotti, K. L., and Okabe, S.: Dual nitrogen and oxygen
552 isotope fractionation during anaerobic ammonium oxidation by anammox bacteria, *ISME Journal*, 13, 2426–2436,
553 <https://doi.org/10.1038/s41396-019-0440-x>, 2019.
- 554 Koeve, W. and Kähler, P.: Heterotrophic denitrification vs. autotrophic anammox-quantifying collateral effects on the
555 oceanic carbon cycle, *Biogeosciences*, 7, 2327–2337, <https://doi.org/10.5194/bg-7-2327-2010>, 2010.
- 556 Kuenen, J. G. and Robertson, L. A.: Ecology of Nitrification and Denitrification-Book.Pdf, in: *The Nitrogen and Sulphur
557 Cycles*, edited by: Cole, J. A. and Ferguson, S., Cambridge University Press, 162–218, 1987.
- 558 Kuypers, M. M. M., Silekers, A. O., Lavik, G., Schmid, M., Jørgensen, B. B., Kuenen, J. G., Sinninghe Damsté, J. S.,
559 Strous, M., and Jetten, M. S. M.: Anaerobic ammonium oxidation by anammox bacteria in the Black Sea, *Nature*, 422, 608–
560 611, <https://doi.org/10.1038/nature01472>, 2003.
- 561 Laffoley, D. and Baxter, J. M.: Ocean deoxygenation : everyone’s problem. Summary for policy makers,
562 <https://doi.org/10.2305/iucn.ch.2019.14.en>, 2019.
- 563 Lembke-Jene, L., Tiedemann, R., Nürnberg, D., Gong, X., and Lohmann, G.: Rapid shift and millennial-scale variations in
564 Holocene North pacific intermediate water ventilation, *Proc Natl Acad Sci U S A*, 115, 5365–5370,
565 <https://doi.org/10.1073/pnas.1714754115>, 2018.



- 566 Liu, Z., Altabet, M. A., and Herbert, T. D.: Glacial-interglacial modulation of eastern tropical North Pacific denitrification
567 over the last 1.8-Myr, *Geophys Res Lett*, 32, 1–4, <https://doi.org/10.1029/2005GL024439>, 2005.
- 568 Lyle, M., Koizumi, I., Richter, C., Fox, P. J., Baldauf, J., and Francis, T. J. G.: Proceedings of the Ocean Drilling Program,
569 <https://doi.org/10.1097/BLO.0b013e3181576080>, 1997.
- 570 Menviel, L., Timmermann, A., Timm, O. E., and Mouchet, A.: Deconstructing the Last Glacial termination: The role of
571 millennial and orbital-scale forcings, *Quat Sci Rev*, 30, 1155–1172, <https://doi.org/10.1016/j.quascirev.2011.02.005>, 2011.
- 572 Nicholson, S. E. and Flohn, H.: African climatic changes in late Pleistocene and Holocene and the general atmospheric
573 circulation., Sea level, ice and climatic change. Proc. Canberra symposium, December 1979, 2, 295–301, 1981.
- 574 Okazaki, Y., Timmermann, A., Menviel, L., Harada, N., Abe-Ouchi, A., Chikamoto, M. O., Mouchet, A., and Asahi, H.:
575 Deepwater Formation in the North Pacific During the last Glacial Termination, *Science* (1979), 329, 200–204, 2010.
- 576 Ortiz, J., Mix, A., Hostetler, S., and Kashgarian, M.: The California Current of the Last Glacial Maximum: Reconstruction at
577 42°N based on multiple proxies, *Paleoceanography*, 12, 191–205, <https://doi.org/10.1029/96PA03165>, 1997.
- 578 Paulmier, A. and Ruiz-Pino, D.: Oxygen minimum zones (OMZs) in the modern ocean, *Prog Oceanogr*, 80, 113–128,
579 <https://doi.org/10.1016/j.pocean.2008.08.001>, 2009.
- 580 Peng, X., Fuchsman, C. A., Jayakumar, A., Oleynik, S., Martens-Habbema, W., Devol, A. H., and Ward, B. B.: Ammonia
581 and nitrite oxidation in the Eastern tropical North Pacific, *Global Biogeochem Cycles*, 29, 2034–2049,
582 <https://doi.org/10.1002/2015GB005278>, 2015.
- 583 Peters, B., Horak, R., Devol, A., Fuchsman, C., Forbes, M., Mordy, C. W., and Casciotti, K. L.: Estimating fixed nitrogen
584 loss and associated isotope effects using concentration and isotope measurements of NO₃⁻, NO₂⁻, and N₂ from the Eastern
585 Tropical South Pacific oxygen deficient zone, *Deep Sea Res 2 Top Stud Oceanogr*, 156, 121–136,
586 <https://doi.org/10.1016/j.dsr2.2018.02.011>, 2018.
- 587 Pierce, S. D., Barth, J. A., Kipp Shearman, R., and Erofeev, A. Y.: Declining oxygen in the northeast Pacific, *J Phys*
588 *Oceanogr*, 42, 495–501, <https://doi.org/10.1175/JPO-D-11-0170.1>, 2012.
- 589 Placencia, J. A., Garcés-Vargas, J., Lange, C. B., and Hebbeln, D.: Alkenone-based temperature patterns along the eastern
590 South Pacific Coastal Ocean: the effect of upwelling and advection on the sedimentary alkenone unsaturation-index
591 (U_{37K}[']), *Biogeosciences Discussions*, 7, 545–564, 2010.



- 592 Rattray, J. E., Van De Vossenberg, J., Hopmans, E. C., Kartal, B., Van Niftrik, L., Rijpstra, W. I. C., Strous, M., Jetten, M.
593 S. M., Schouten, S., and Damsté, J. S. S.: Ladderane lipid distribution in four genera of anammox bacteria, *Arch Microbiol*,
594 190, 51–66, <https://doi.org/10.1007/s00203-008-0364-8>, 2008.
- 595 Rattray, J. E., Van Vossenberg, J. De, Jaeschke, A., Hopmans, E. C., Wakeham, S. G., Lavik, G., Kuypers, M. M. M.,
596 Strous, M., Jetten, M. S. M., Schouten, S., and Sinninghe Damsté, J. S.: Impact of temperature on ladderane lipid distribution
597 in anammox bacteria, *Appl Environ Microbiol*, 76, 1596–1603, <https://doi.org/10.1128/AEM.01796-09>, 2010.
- 598 Reid, J. L.: On the total geostrophic circulation of the pacific ocean : flow patterns , tracers , and transports , 39, 263–352,
599 1997.
- 600 Reid, J. L. and Mantyla, A. W.: On the Mid-Depth Circulation of the North Pacific Ocean, *J Phys Oceanogr*, 8, 946–951,
601 [https://doi.org/10.1175/1520-0485\(1978\)008<0946:otmdco>2.0.co;2](https://doi.org/10.1175/1520-0485(1978)008<0946:otmdco>2.0.co;2), 1978.
- 602 Robinson, R. S., Kienast, M., Albuquerque, A. L., Altabet, M., Contreras, S., Holz, R. D. P., Dubois, N., Francois, R.,
603 Galbraith, E., Hsu, T., Ivanochko, T., Jaccard, S., Kao, S., Kiefer, T., Kienast, S., Lehmann, M., Martinez, P., Mccarthy, M.,
604 Möbius, J., Pedersen, T., Quan, T. M., Ryabenko, E., Schmittner, A., Schneider, R., and Schneider-mor, A.: A review of
605 nitrogen isotopic alteration in marine sediments, 27, <https://doi.org/10.1029/2012PA002321>, 2012.
- 606 Rush, D. and Sinninghe Damsté, J. S.: Lipids as paleomarkers to constrain the marine nitrogen cycle, *Environ Microbiol*, 19,
607 2119–2132, <https://doi.org/10.1111/1462-2920.13682>, 2017.
- 608 Rush, D., Jaeschke, A., Hopmans, E. C., Geenevasen, J. A. J., Schouten, S., and Damsté, J. S. S.: Short chain ladderanes:
609 Oxid biodegradation products of anammox lipids, *Geochim Cosmochim Acta*, 75, 1662–1671,
610 <https://doi.org/10.1016/j.gca.2011.01.013>, 2011.
- 611 Rush, D., Wakeham, S. G., Hopmans, E. C., Schouten, S., and Sinninghe Damsté, J. S.: Biomarker evidence for anammox in
612 the oxygen minimum zone of the Eastern Tropical North Pacific, *Org Geochem*, 53, 80–87,
613 <https://doi.org/10.1016/j.orggeochem.2012.02.005>, 2012a.
- 614 Rush, D., Hopmans, E. C., Wakeham, S. G., Schouten, S., and Damst, J. S. S.: Occurrence and distribution of ladderane
615 oxidation products in different oceanic regimes, 2407–2418, <https://doi.org/10.5194/bg-9-2407-2012>, 2012b.
- 616 Rush, D., Hopmans, E. C., Wakeham, S. G., Schouten, S., and Sinninghe Damsté, J. S.: Occurrence and distribution of
617 ladderane oxidation products in different oceanic regimes, *Biogeosciences*, 9, 2407–2418, [https://doi.org/10.5194/bg-9-](https://doi.org/10.5194/bg-9-2407-2012)
618 2407-2012, 2012c.



- 619 Rush, D., Talbot, H. M., Van Der Meer, M. T. J., Hopmans, E. C., Douglas, B., and Damsté, J. S. S.: Biomarker evidence for
620 the occurrence of anaerobic ammonium oxidation in the eastern Mediterranean Sea during Quaternary and Pliocene sapropel
621 formation, *Biogeosciences*, 16, 2467–2479, <https://doi.org/10.5194/bg-16-2467-2019>, 2019.
- 622 Ryabenko, E.: Stable Isotope Methods for the Study of the Nitrogen Cycle, in: *Topics in Oceanography*, edited by:
623 Zambianchi, E., 49–88, <https://doi.org/10.5772/56105>, 2013.
- 624 Sahu, S., Allen, S. E., Saldías, G. S., Klymak, J. M., and Zhai, L.: Spatial and Temporal Origins of the La Perouse Low
625 Oxygen Pool: A Combined Lagrangian Statistical Approach, *J Geophys Res Oceans*, 127, 1–20,
626 <https://doi.org/10.1029/2021JC018135>, 2022.
- 627 Sigman, D. M. and Fripiat, F.: Nitrogen isotopes in the ocean, in: *Encyclopedia of Ocean Sciences*, edited by: Kirk Cochran,
628 J., Bokuniewicz, H. J., and Yager, P. L., Elsevier Ltd, 263–278, <https://doi.org/10.1016/B978-0-12-409548-9.11605-7>, 2019.
- 629 Sinninghe Damsté, J. S., Strous, M., Rijpstra, W. I. C., Hopmans, E. C., Geenevasen, J. A. J., Van Duin, A. C. T., Van
630 Niftrik, L. A., and Jetten, M. S. M.: Linearly concatenated cyclobutane lipids form a dense bacterial membrane, *Nature*, 419,
631 708–712, <https://doi.org/10.1038/nature01067>, 2002.
- 632 Smith, K. L., Messié, M., Connolly, T. P., and Huffard, C. L.: Decadal Time-Series Depletion of Dissolved Oxygen at
633 Abyssal Depths in the Northeast Pacific, *Geophys Res Lett*, 49, <https://doi.org/10.1029/2022GL101018>, 2022.
- 634 Sollai, M., Hopmans, E. C., Schouten, S., Keil, R. G., and Sinninghe Damsté, J. S.: Intact polar lipids of Thaumarchaeota
635 and anammox bacteria as indicators of N cycling in the eastern tropical North Pacific oxygen-deficient zone,
636 *Biogeosciences*, 12, 4725–4737, <https://doi.org/10.5194/bg-12-4725-2015>, 2015.
- 637 Sonnerup, R. E., Quay, P. D., and Bullister, J. L.: Thermocline ventilation and oxygen utilization rates in the subtropical
638 North Pacific based on CFC distributions during WOCE, *Deep Sea Res 1 Oceanogr Res Pap*, 46, 777–805,
639 [https://doi.org/10.1016/S0967-0637\(98\)00092-2](https://doi.org/10.1016/S0967-0637(98)00092-2), 1999.
- 640 Stramma, L., Johnson, G. C., Firing, E., and Schmidtko, S.: Eastern Pacific oxygen minimum zones: Supply paths and
641 multidecadal changes, *J Geophys Res Oceans*, 115, 1–12, <https://doi.org/10.1029/2009JC005976>, 2010.
- 642 Tesdal, J. E., Galbraith, E. D., and Kienast, M.: Nitrogen isotopes in bulk marine sediment: Linking seafloor observations
643 with subseafloor records, *Biogeosciences*, 10, 101–118, <https://doi.org/10.5194/bg-10-101-2013>, 2013.



- 644 Thamdrup, B., Dalsgaard, T., Jensen, M. M., Ulloa, O., Farías, L., and Escribano, R.: Anaerobic ammonium oxidation in the
645 oxygen-deficient waters off northern Chile, *Limnol Oceanogr*, 51, 2145–2156, <https://doi.org/10.4319/lo.2006.51.5.2145>,
646 2006.
- 647 Thomson, R. E. and Krassovski, M. V.: Poleward reach of the California Undercurrent extension, *J Geophys Res Oceans*,
648 115, <https://doi.org/10.1029/2010JC006280>, 2010.
- 649 Thunell, R. C. and Kepple, A. B.: Glacial-Holocene D15N record from the Gulf of Tehuantepec, Mexico: Implications for
650 denitrification in the eastern equatorial Pacific and changes in atmospheric N₂O, *Global Biogeochem Cycles*, 18,
651 <https://doi.org/10.1029/2002GB002028>, 2004.
- 652 Vallero, D. A.: Air pollution biogeochemistry, in: *Air Pollution Calculations*, edited by: Vallero, D. A., Elsevier, 175–206,
653 <https://doi.org/10.1016/b978-0-12-814934-8.00008-9>, 2019.
- 654 Wang, Y., Hendy, I. L., and Zhu, J.: Expansion of the Southern California oxygen minimum zone during the early-to mid-
655 Holocene due to reduced ventilation of the Northeast Pacific, *Quat Sci Rev*, 238, 106326,
656 <https://doi.org/10.1016/j.quascirev.2020.106326>, 2020.
- 657 Ward, B. B.: How Nitrogen Is Lost, 341, 352–354, 2013.
- 658 White, M. E., Rafter, P. A., Stephens, B. M., Wankel, S. D., and Aluwihare, L. I.: Recent Increases in Water Column
659 Denitrification in the Seasonally Suboxic Bottom Waters of the Santa Barbara Basin, *Geophys Res Lett*, 46, 6786–6795,
660 <https://doi.org/10.1029/2019GL082075>, 2019.
- 661 Whitney, F. A., Freeland, H. J., and Robert, M.: Persistently declining oxygen levels in the interior waters of the eastern
662 subarctic Pacific, *Prog Oceanogr*, 75, 179–199, <https://doi.org/10.1016/j.pocean.2007.08.007>, 2007.
- 663 Zhou, Y., Gong, H., and Zhou, F.: Responses of Horizontally Expanding Oceanic Oxygen Minimum Zones to Climate
664 Change Based on Observations, *Geophys Res Lett*, 49, 1–11, <https://doi.org/10.1029/2022GL097724>, 2022.
- 665 Zonneveld, K. A. F., Versteegh, G. J. M., Kasten, S., Eglinton, T. I., Emeis, K., Huguet, C., and Koch, B. P.: Selective
666 preservation of organic matter in marine environments ; processes and impact on the sedimentary record, 483–511, 2010.
- 667
- 668